Journal of
Materials Chemistry C

Materials for optical, magnetic and electronic devices
rsc.li/materials-c

Volume 6
Number 5
7 February 2018
Pages 911-1266

ISSN 2050-7526

ROYAL SOCIETY OF CHEMISTRY

PAPER
Nosang V. Myung, Yong-Ho Choa *et al.*
A noble gas sensor platform: linear dense assemblies of single-walled carbon nanotubes (LACNTs) in a multi-layered ceramic/metal electrode system (MLES)

This is an Accepted Manuscript, which has been through the Royal Society of Chemistry peer review process and has been accepted for publication.

Accepted Manuscripts are published online shortly after acceptance, before technical editing, formatting and proof reading. Using this free service, authors can make their results available to the community, in citable form, before we publish the edited article. We will replace this Accepted Manuscript with the edited and formatted Advance Article as soon as it is available.

You can find more information about Accepted Manuscripts in the Information for Authors.

Please note that technical editing may introduce minor changes to the text and/or graphics, which may alter content. The journal's standard Terms & Conditions and the Ethical guidelines still apply. In no event shall the Royal Society of Chemistry be held responsible for any errors or omissions in this Accepted Manuscript or any consequences arising from the use of any information it contains.

ROYAL SOCIETY OF CHEMISTRY

rsc.li/materials-c

REVIEW

High performance narrow-band green-emitting phosphors for white LEDs: recent advances and perspectives

Yujia Wan,[ab] Dongjie Liu,[a] Wei Yang,[ab] Yingsheng Wang,[ab] Min Zhang,[ab] Hongzhou Lian, *[a] Peipei Dang,*[a] Guogang Li,*[c] and Jun Lin*[ab]

Ultra-wide color gamut backlight is the key to achieve ultra-high definition and ultra-high resolution liquid crystal display (LCD), in which green-emitting phospohrs with narrow spectral emission are the decisive factors. However,the key green-emitting phosphors currently used for light emitting diode (LED) backlights, shch as commercial β-SiAlON:Eu^{2+}, has the disadvantages of wide emission band and large particles. In order to display more colorful and vivid photograph, it's urgent to accelerate the development of narrow-band green-emitting phosphr with independent intellectual property rights and high quantum efficiency. This article outlines the design of green-emitting phosphors and the improvement of their luminescent properties. From design aspect, an excellent phosphor should consider host and activator. The emission band of Tb^{3+}, Mn^{2+}, Ce^{3+} and Eu^{2+} usually located in the visible region, and the short luminesce decay time of Eu^{2+}/Ce^{3+} makes Eu^{2+}/Ce^{3+} as the potential activator for high-quality display. For selecting the host, single particle diagnosis approach, high-throughput density functional theory (DFT) calculation and mineral-inspired prototype evolution are used to explore novel phosphors. The thermal stability and quantum efficiency (QE) are the important properties and their enhancing strategies are presented. Moreover, the color gamut of many green-emitting phosphors is shown and the green-emitting phosphor-based WLEDs are used in LCD screen and projector, which shows more vivid pictures than commercial WLED. Finally, the future outlook of how to explore green-emitting phosphors with better perfomance was discussed.

1. Introduction

High-definition display as a display media has been an essential part in daily life such as television, computer display and cellphone.[1,2] The backlight that provides light source to display image decides the richness of the display color in an image. A variety of display types such as backlight in liquid crystal display (LCD), organic light emitting diode (OLED), quantum dot LED (QLED) and Micro-LED with favorable luminescence performance have been widely concerned and studied.[3–8] OLED, QLED and Micro-LED as novel approaches to achieve white light has a lot of advantages, such as higher brightness, higher efficiency and lower power consumption, however, there are a lot of drawbacks.[9–13] OLED has high response time and large color gamut, but its short lifetime, poor thermal stability and high cost limit its further usage. Cd-based QD as a component of QLED is unstable in humid environment, and the Cd will harm to environment.[14] The high cost of Micro-LED's hinders its

further development in practical application.[15–19] Phosphor-converted white LED (pc-WLED) is usually used to fabricated backlight in LCD for its long lifetime, low energy consumption and less cost.[20–22] Hence, backlight in LCD as a reliable and mature technique was put into practice application under the comprehensive consideration.[23–27]

The commercial backlight in LCD is pc-WLED fabricated by GaN blue chip + narrow-band green β-SiAlON:Eu^{2+} (β-SiAlON) and linear red emission K$_2$SiF$_6$:Mn^{4+} (KSF:Mn^{4+}) phosphors.[28] The level of backlighting used to display color can be measured by the color gamut, which is the area of the triangle made up of the CIE coordinates of the red-, green-, and blue-emitting phosphors. The larger the triangle area is, the more colors can be displayed, representing the high-quality display. In order to acquire more realistic display patterns, the color gamut should be further expanding. The blue and red emission coordinates formed by GaN chip of (0.141, 0.042) and KSF:Mn^{4+} phosphor of (0.692, 0.308) are very close to the bule and red edge of the gamut diagram, respectively. β-SiAlON as a commercial phosphor emits intense green light peaking at 538 nm with FWHM of 48 nm and exhibits high internal quantum efficiency/absorption (IQE/Abs) of 91%/66%.[29] Moreover, β-SiAlON has good chemical and physical stability, showing the long working life in practical application. Xie's group developed a synthetic method of β-SiAlON, which uses the mechanical grinding and acid washing processes, efficiently improving the IQE to 79% even at small particle size of 3.13 μm.[30] This enhancement allows β-SiAlON to be used in mini-LED, providing

a. State Key Laboratory of Rare Earth Resource Utilization
Changchun Institute of Applied Chemistry, Chinese Academy of Sciences
Changchun, Jilin 130022, P. R. China
Email: ppdang@ciac.ac.cn; hzlian@ciac.ac.cn; jlin@ciac.ac.cn

b. School of Applied Chemistry and Engineering
University of Science and Technology of China
Hefei, Anhui 230026, P. R. China

c. Faculty of Materials Science and Chemistry
China University of Geosciences
Wuhan, Hubei 430074, P. R. China
Email: ggli@cug.edu.cn

a new solution for high-definition display. However, owing to the bandwidth and peak position, the green coordinate calculated by commercial β-SiAlON phosphor is (0.244, 0.633), which has room for improvement. Narrower green-emitting phosphor should be explored, whose color coordinate can be extended to the edge of gamut diagram. More than that, the luminescence thermal stability of phosphors should be focused, it is important to maintain original intensity at high temperature. The β-SiAlON suffers from poor luminescence thermal stability, it only maintains 88% integrated intensity at 423 K, which should be further improved. It is preferable to develop phosphors with zero thermal quenching. The brightness of display will not decay after long worktime. The researchers put forward a lot of methods to enhance the thermal stability, such as adding flux, cation substitution and mineral-inspired evolution. Therefore, developing novel green phosphor with narrow-band and good thermal stability is a key demand in backlight display.[31,32]

In this review, we first select activators based on classic visible emission of Mn^{2+}, Ce^{3+}, Eu^{2+}, Tb^{3+} and host based on three feasible ways (single particle diagnosis approach, high-throughput DFT calculation, and mineral-inspired prototype evolution). Then, multiple methods of modulating luminescence and enhancing the luminescence thermal stability and QE are presented. The color gamut of green-emitting based LED was further compared and the practicability was examined by kinds of application. On the end, we discuss the futural development perspective of green-emitting phosphors, the green-emitting phosphors should focus on small particle size with high QE and thermal stability which can used in mini-LED or Micro-LED. The theoretical study of negative thermal quenching and abnormal luminescent situation should be further explored, and the theoretical selection of green-emitting phosphors with good performance should be established.

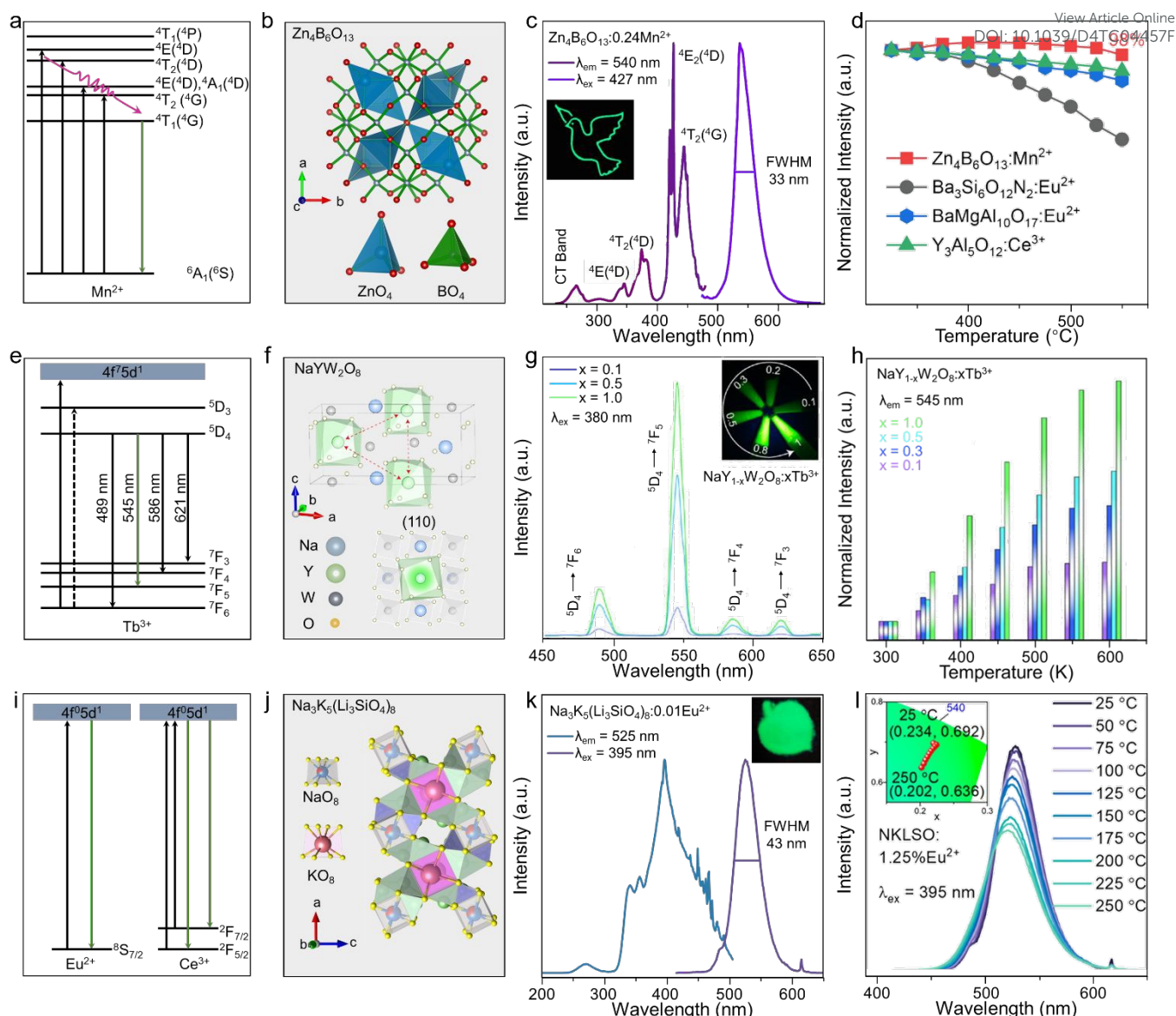## 2. Design of green-emitting phosphor

2.1 Activator selection of green-emitting phosphor

A green-emitting phosphor should meet the requirements of specific peak position (492~577 nm), narrow-band emission with FWHM less than 60 nm. To expand the color gamut, the band width should be narrower and the position should be better in the range of 520-530 nm. Based on these requirements, an excellent green-emitting phosphor should have high luminescence efficiency, high thermal stability and short luminescence decay time, which will contribute to practical display application. From a design perspective, an inorganic phosphor includes host and luminescence center, both have a great influence on luminescence performance. The Mn^{2+}, Ce^{3+}, Eu^{2+}, Tb^{3+} are selected as the luminescence centers of green phosphor due to their emission bands usually located in the visible region. Different host and intrinsic electronic structure properties will produce different luminescence, so that green-emitting phosphors can be designed directionally.

Transition mental Mn^{2+} belongs to parity and spin-forbidden transition of d-d ($^4T_1 \rightarrow {}^6A_1$), however, the electronic transition will couple the part of parity-allowed vibrations, making the emission band to be broadband (Figure 1a).[33,34] The outer d orbital is significantly affected by the local environment, therefore, the emission band mainly depends on the host structure.[35,36] The Mn^{2+} exhibits green emission after located in the weak crystal-field (tetrahedral coordination), therefore, a lot of Mn^{2+}-doped green-emitting phosphors were designed.[37,38] $Zn_4B_6O_{13}$ exhibits tetrahedral coordinated lattice ZnO_4 and BO_4 (Figure 1b). Mn^{2+} in $Zn_4B_6O_{13}$ emits green light peaking at 540 nm with FWHM of 33 nm (Figure 1c) and shows near zero thermal quenching (ZTQ), which maintains 103% initial intensity at 150 °C (Figure 1d).[39] The symmetry space group $I\bar{4}3m$ and rigid structure contribute to the good thermal stability. However, Mn^{2+}-doped phosphors have some intrinsic drawbacks, owing to the spin-forbidden transition. The excitation peak is narrow and the absorption is low, resulting in low quantum efficiency. Moreover, the Mn^{2+}-doped phosphors has relative long decay time of several ms, inducing the sticking image, which is not suitable for high quality display with high refresh rate.

The rare earth ion Tb^{3+} exhibits green emission due to the intrinsic electronic transition which belongs to parity-forbidden transition of 4f - 4f, and the 4f electron is shielded by the outer electron orbit of 5s, therefore, the emission spectrum is difficult to effected by local structure and shows the intrinsic emission of Tb^{3+}.[40,41] The detailed emission transition of Tb^{3+} is $^5D_4 \rightarrow {}^7F_J$ (J = 3, 4, 5 and 6), which is presented as line emission and mainly locates in the green region (Figure 1e).[42,43] Tb^{3+}-doped green-emitting phosphors have been widely studied, for example, $NaYW_2O_8$:Tb^{3+} has main green emission peaking at 545 nm and its main excitation peaks range from 200-400 nm, and heavy concentration of Tb^{3+} can enhance PL intensity.(Figure 1f and 1g). Moreover, Tb^{3+} shows good thermal stability in $NaYW_2O_8$, it can reach highest 20-fold under the excitation at 412 nm. (Figure 1h).[44] However, due to the 4f-5d allowed transition of Tb^{3+} in excitation, the intensity of 4d-5d excitation band is stronger than the other 4f-4f forbidden transition.[45] The characteristic excitation band of Tb^{3+} is located range from 200 to 300 nm induced by 4f-5d allowed transition and becomes main excitation band. It is obvious that the Tb^{3+} singly-activated phosphors are usually excited by n-UV light, there are few Tb^{3+}-doped phosphors excited by blue light which limits its display application. A conventional strategy for that to expand the excitation band and enhance luminescence quantum is adding sensitizers such as Ce^{3+}, Pr^{3+} and Sm^{3+}.[46–48] The energy transfer to Tb^{3+} is achieved by utilizing the intense emission of Ce^{3+} in $Ca_2GdHf_2Al_3O_{12}$, a green-emitting phosphor $Ca_2GdHf_2Al_3O_{12}$:Tb^{3+},Ce^{3+} exhibits 543 nm emission with high IQE/EQE of 83%/66%.[49] Whereas, because of 4f-4f forbidden transition in emission, the luminescence lifetime of Tb^{3+} also reaches ms-level, which is not conducive to high-definition display. Due to the relatively low luminescence efficiency induced by f-f transition and the difficulty of Tb^{3+} excited by blue chips for Tb^{3+}-doped phosphors, their application is hindered.

Figure 1. (a) The energy level diagram of Mn^{2+} and the purple line represents nonradiative transition. (b) The crystal structure of $Zn_4B_6O_{13}$ and the coordination polyhedra of ZnO_4 and BO_4, the red ball represents the O atom. (c) The PL and PLE spectra of $Zn_4B_6O_{13}:Mn^{2+}$. (d) The nearly ZTQ property of $Zn_4B_6O_{13}:Mn^{2+}$. (e) The energy level diagram of Tb^{3+}. (f) The crystal structure of $NaYW_2O_8$, the bule, green, gray and yellow balls represent the Na, Y, W and O, respectively. (g) The PL spectra of $NaYW_2O_8:xTb^{3+}$. (h) The anti-TQ property of $NaYW_2O_8:xTb^{3+}$. (i) The energy level diagram of Eu^{2+} and Ce^{3+}. (j) The crystal structure of $Na_3K_5(Li_3SiO_4)_8$ and the coordination polyhedra of NaO_8 and KO_8. (k) The PL and PLE spectra of $Na_3K_5(Li_3SiO_4)_8:Eu^{2+}$. (l) The TQ property of $Na_3K_5(Li_3SiO_4)_8:Eu^{2+}$. Reproduced with permission from ref. 36. Copyright 2021, Elsevier, ref. 40. Copyright 2023, Wiley and ref. 26. Copyright 2023, American Chemical Society.

Rare earth ions Eu^{2+} and Ce^{3+} with 4f-5d parity-allowed transition have attracted extensive attention for tuning band width from ten to hundreds of nanometers (Figure 1i).[50–56] The outer sphere 5d orbital is more susceptible to the crystal field than 4f orbital. Hence, the band shape and width of a phosphor can be adjusted through modifying crystal field environment. Benefiting from the allowed optical transition of 4f-5d transition, the emission and excitation band are band-shape, which usually has a high luminous efficiency. Whereas Ce^{3+} is not suitable as an activator for narrow-band emission phosphor, the 4f ground state of Ce^{3+} is split to two energy levels which result relative broad-band emission. The excitation of Eu^{2+}-

doped phosphor usually located in n-UV region and the spectrum of that usually exhibits broad-band emission which induced by the allowed 4f-5d transition, hence, the host of Eu^{2+} should be carefully selected. For the promising Eu^{2+} activator doped in the host, high symmetry lattice and coordination number are more likely to achieve green emission, the eight-coordinated cube and distorted cube usually show the cyan to green emission. A lot of Eu^{2+}-doped green-emitting phosphors were developed with good performance. $Na_3K_5(Li_3SiO_4)_8:Eu^{2+}$ ($N_3K_5:Eu^{2+}$) emits intense green light peaking at 525 nm with FWHM of 43 nm (Figure 1j and 1k), and shows high thermal stability and IQE. It's integrated intensity maintains 96% at 150

°C compared to room temperature (Figure 1l), and its IQE is enhanced to near 100% after adding the Al^{3+} as charge compensator.[29] The PL decay time of Eu^{2+} usually exhibits ns–level, which is more suitable for display with high refresh rates. However, the Eu and Ce normally exit in the form Eu^{3+} and Ce^{4+}, respectively, the Eu^{2+} and Ce^{3+} are usually reduced in the reducing gas at sintering temperature. The synthesis condition of Eu^{2+} and Ce^{3+} is more complicated than Tb^{3+} and Mn^{2+}. Moreover, owing the two 4f energy level ($^2F_{2/7}$ and $^2F_{2/5}$) of Ce^{3+}, the emission of Ce^{3+} always exhibits two peaks, which is broader than Eu^{2+}.

2.2 Host selection of green-emitting phosphor

It is a tedious process to use the traditional artificial trial and error method to explore new phosphors, which will consume a lot of money and time. Moreover, the luminescent properties of new phosphors, such as peak position and width, may not meet the actual needs, resulting in slow exploration of specific green-emitting phosphors. To meet the specific wavelength requirements and achieve customized green phosphors, there are three feasible ways: 1) single particle diagnosis approach, 2) high-throughput density functional theory (DFT) calculation and 3) mineral-inspired prototype evolution. These methods have been extensively understood and used to explore novel phosphors (Figure 2a).

The first method is single particle diagnosis approach. Same luminescent center such as Eu^{2+} and Ce^{3+} may has various emission after doping into different host. The powder sample is usually synthesized as mixture phase with different luminescence. It's difficult to observe the detailed luminescence and pure phase at the same time. Single particle diagnosis approach can select the targeted luminescence after the powder is amplified to a single powder particle.[57,58] The particle sample will be explored by single crystal XRD and single particle fluorescence spectroscopy system. Finally, the powder phosphor will be synthesized after identifying composition.[59] Xie's group explored a narrow-band green-emitting Ba$_2$LiSi$_7$AlN$_{12}$:Eu^{2+} phosphor by single particle diagnosis, and the particle emits green light under UV light, as shown in the Figure 2b and 2c. Ba$_2$LiSi$_7$AlN$_{12}$:Eu^{2+} shows green luminescence peaking at 515 nm with FWHM of 61 nm due to the symmetric lattice occupied by Eu^{2+} (Figure 2d and 2e).[60]

The theoretical method is identified as a highly efficient approach for developing new phosphors with specified optical properties, which spends less time than elaborate trial-and-error process.[61–63] High-throughput DFT calculation is usually considered as a practical method for selecting targeted phosphors. Rami et al. proposed descriptors related to emission energy position and bandwidth of Eu^{2+}-doped phosphors. Since the emission spectrum of Eu^{2+} mainly depends on the 4f-5d transition process and is greatly affected by the 5d orbits. The (anti) bonding interaction between Eu^{2+} and ligands in 5d excited orbitals is proportional to excited state distortion. A group of phosphors SrMg$_3$SiN$_4$:Eu^{2+} (SMS), BaMg$_3$SiN$_4$:Eu^{2+} (BMS), SrLiAl$_3$N$_4$:Eu^{2+} (SLA), CaLiAl$_3$N$_4$:Eu^{2+} (CLA), SrAl$_2$Li$_2$O$_2$N$_2$:Eu^{2+} (SALON), and SrLi$_2$Be$_4$N$_6$:Eu^{2+} (SLBO) with similar structure were taken to construct an experimental law.

By using the band width as a function of the covalency coefficient α^2 of the acceptor Eu 5d MO in the emission process, a linear relation is fitted by the research between experimental emission peak and computed absorption energy maximum of band (Figure 2f and 2g). Based on the above analysis, high-level wavefunction-based *ab* initio quantum chemistry combines with time-dependent density functional theory (TD-DFT) and an excited-state dynamics (ESD) approach were used to develop a protocol for predicting the emission energy position and bandwidth of Eu^{2+}-doped phosphors (Figure 2h).[64] Moreover, the host of a narrow-band emission phosphor can be directly selected in the crystal structure database (Figure 2i). First, specific optical properties should be determined, such as narrow-band, green emission and good thermal stability, then a series of descriptors were proposed such as host band gap, host band structure and Debye temperature. Secondly, the specific descriptor values are determined by comparing the experimental data. Then, the specific descriptor values of phosphors in crystal structure database were calculated and the phosphors with target conditions will be selected. For example, the Debye temperature can be used to indicate the strength of the structure rigidity, the formular of that is shown in the following:
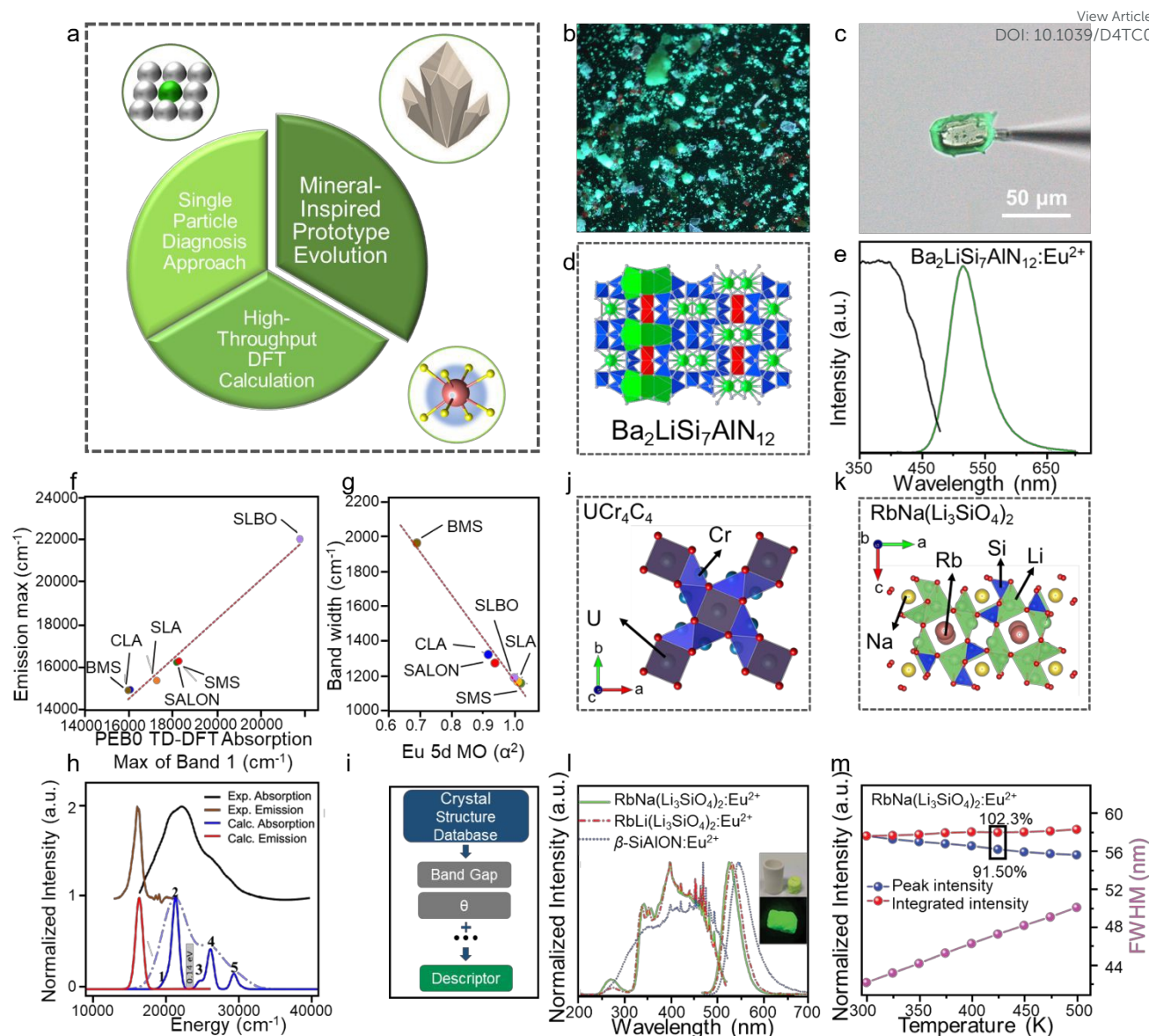
$$\Theta = \frac{\hbar}{k}\left[6\pi^2 V^{\frac{1}{2}} N\right]^{\frac{1}{3}}\sqrt{\frac{B_H}{M}}f(\nu) \qquad \text{equation (1)}$$

$$f(\nu) = \left\{3\left[2\left(\frac{2}{3}\frac{1+\nu}{1-2\nu}\right)^{3/2} + \left(\frac{1}{3}\frac{1+\nu}{1-\nu}\right)^{3/2}\right]^{-1}\right\}^{1/3} \qquad \text{equation (2)}$$

where $\hbar$ is Plank constant, M is the molecular mass of chemical formula, k is the Bolatzmann constant, N is the number of atoms in one unit cell, B$_H$ is the bulk modulus of crystal, V is the volume of unit cell and ν is Poisson ratio which is related to the lateral deformation coefficient of crystal.[83] The higher the Debye temperature is, the stronger the rigidity is. The commercial green-emitting *β*-SiAlON phosphor has relatively good luminescence thermal stability. The Debye temperature of phosphors can be obtained by both experiment and calculation. When the Debye temperature of the phosphors is higher than that of *β*-SiAlON, presenting the phosphors have better thermal stability.

The final method to design new phosphors is mineral-inspired prototype evolution based on specific mineral structure derivation such as UCr$_4$C$_4$-type or garnet-type.[65,66] Through changing the atoms in a certain compound composition, the same or similar structure can be obtained, which further getting the similar good luminescence properties. Taking UCr$_4$C$_4$-type as example, the composition Me(A, B)$_4$X$_4$ is consist of alkali metal and alkaline earth metal ions Me, [AX$_4$] and [BX$_4$] tetrahedra connect with each other by common edges or vertices. Me ions are located in the framework to form the rigid structure with the density κ = (AB/X) = 1. UCr$_4$C$_4$-type materials have stable and rigid structure, as well as cubic-like lattice. The high rigidity structure can reduce nonradiative transition, and the symmetric lattice site is easier to emit narrow-band emission (Figure 2j).[67–69] Due to the relative lower electronegativity and larger nephelauxetic effect of N in nitride than that of O in oxide,

Figure 2. (a) The schematic diagram of three approaches: single particle diagnosis approach, mineral-inspired prototype evolution and high-throughput DFT calculation. (b) The picture of product synthesized by the mixture of Ba, Si, Al, Li and Eu. (c) The green-emitting particle selected by the single particle diagnosis approach. (d) The crystal structure of $Ba_2LiSi_7AlN_2$. (e) The PL and PLE spectra of $Ba_2LiSi_7AlN_2:Eu^{2+}$. (f) The wave number of experimental emission peak. (g) The experimental band width of as a function of the covalency coefficient α^2 of the acceptor Eu 5d MO in the emission process for the SMS (green cycle), BMS (brown cycle), SLA (orange cycle), CLA (blue cycle), SALON (red cycle), and SLBO (purple cycle). (h) SMS experimental (black), calculated TD-DFT/PBE0 absorption (blue, light blue) spectra and experimental (brown), and TD-DFT/ PBE0/ESD-calculated (red) emission spectra. (i) The simple flow diagram of selecting the good-performance phosphors. (j) The crystal structure of UCr_4C_4. (k) The crystal structure of $RbNa(Li_3SiO_4)_2$. (l) The PL and PLE spectra of $RbNa(Li_3SiO_4)_2:Eu^{2+}$. (m) The relative peak intensity and integrated intensity at different temperature. Reproduced with permission from ref. 55. Copyright 2015, American Chemical Society, ref. 59. Copyright 2022, American Chemical Society and ref. 65. Copyright 2019, Wiley.

the UCr_4C_4-type nitride phosphors usually exhibit red emission, and oxide phosphors exhibit blue-to-green emission. Xia's group developed a series of UCr_4C_4-type oxide phosphors, among them, $RbNa(Li_3SiO_4)_2:Eu^{2+}$ (RN:Eu^{2+}) phosphor with high rigid structure emits bright green light peaking at 523 nm with FWHM of 41 nm (Figure 2k and 2l). The high rigid and symmetry provide favorable conditions for good PL thermal stability, RN:Eu^{2+} maintains 102% integrated PL intensity at 152 °C (Figure

2m).[70] The single particle diagnosis approach can simplify the pure phase process and reduce the synthesis time, however, this approach requires more sophisticated detected instruments for characterization such as single crystal XRD and single particle fluorescence spectroscopy system. The high-throughput DFT calculation approach can greatly reduce the time of trial-and-error synthesis, whereas,
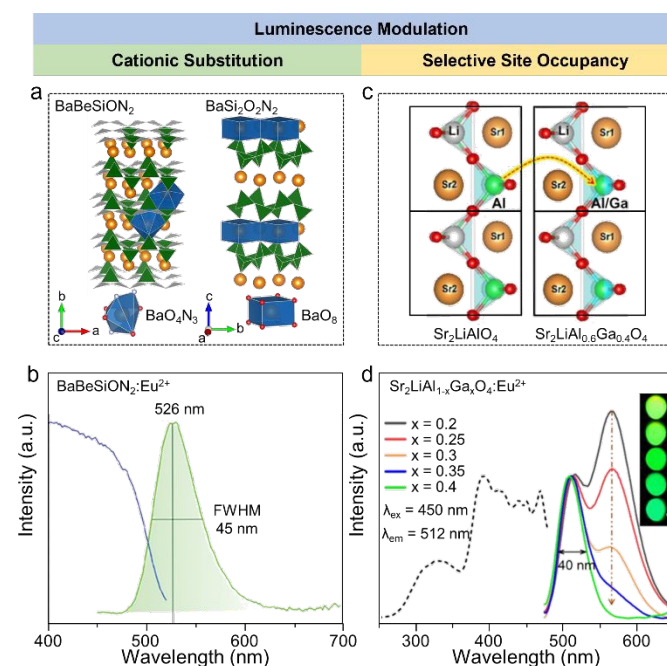
Table 1. Photoluminescence properties of green-emitting UCr_4C_4-type oxide phosphors, including their peak position, FWHM, thermal stability and QE.

Formular	Peak Position (nm)	FWHM (nm)	Thermal Stability (integrated intensity)	Quantum Efficiency	
				IQE	EQE
$RbNa(Li_3SiO_4)_2:Eu^{2+}$	523	41	102%@152°C	96%	44%
$Na_3K_5(Li_3SiO_4)_8:Eu^{2+}$	525	43	96%@150°C	100%	40%
$Rb_3Na(Li_3SiO_4)_4:Eu^{2+}$	527	42	102%@150°C	85%	40%
$NaK_2Li(Li_3SiO_4)_4:Eu^{2+}$	528	44	97%@150°C	81%	51%
$RbLi(Li_3SiO_4)_2:Eu^{2+}$	530	42	103%@150°C	80%	29%
$CsK_2Na(Li_3SiO_4)_4:Eu^{2+}$	531	46	96.3%@150°C	94%	16%

it also needs a lot of time for building computational models and advanced computer for calculation. Compare to them, mineral-inspired prototype evolution becomes a simple and time-saving way to explore new green-emitting phosphors, which can directionally design and synthesize target phosphor by a certain mineral prototype. Among many mineral prototypes, UCr_4C_4-type phosphors with excellent luminescence properties have received wide attention from researchers and several green-emitting phosphors were developed, as shown in Table 1. UCr_4C_4-type oxide phosphors usually exhibit narrow-band green emission peaking around 525 nm with FWHM of less than 50 nm. Benefit from the high structural density and rigidity, the UCr_4C_4-type phosphors have excellent PL thermal stability, all of them maintain >95% integrated PL intensity at 150 °C. Based on the 4f-5d optically allowed transition of Eu^{2+}, their IQEs are relatively higher than that of normal green-emitting phosphors, and their EQEs need to be improved due to the low absorption. Not only that, the microcosmic mechanism of how the rigid structure affects the luminescence is deeply study. Ning's group combines the first-principles and the experimental data about $RbNa(Li_3SiO_4)_2$, conducting that the emission band shape is basically controlled by electron-phonon coupling in $RbNa(Li_3SiO_4)_2$. The insight about emission band width has been put forward. Due to the high rigidity of host, the structural strain caused by electron transition is well distributed. Hence the structural relaxation is weakened, further limiting the emission band broadening.[71] The enhancement of UCr_4C_4-type green-emitting phosphors should focus on absorption enhancement. The following Table 1 lists a series of UCr_4C_4-type oxide green-emitting phosphors with good luminescence properties.[70,72–75]

Although there are many green-emitting phosphors with good luminescence properties, there are still many aspects that should be improved for commercial LEDs. An excellent green-emitting phosphor in display should meet the requirements of ability to expand the color gamut as much as possible, good thermal and chemical stability, high quantum efficiency and simple synthesis method. Hence, it provides inspiration to develop high-quality green-emitting phosphors in display and it can be discussed from three aspects: 1) color gamut, including peak position, FWHM and color purity; 2) stability, including thermal stability and other stability under different working conditions such as high humidity, long usage time and high work current, and 3) high quantum efficiency.

2.3 Luminescence modulation

As mentioned above, the key point of color gamut in display is the CIE color coordinate of green-emitting phosphor, which should close to the edge of the gamut diagram. The color coordinate of phosphor depends on the peak position and FWHM of emission spectrum. The peak position should range from 520 to 530 nm and the FWHM should narrower than 50 nm. The selective conditions of green emission with different activators (Tb^{3+}, Mn^{2+}, Ce^{3+} and Eu^{2+}) have been discussed previously, the development for luminescence modulation should be further explored.[76]

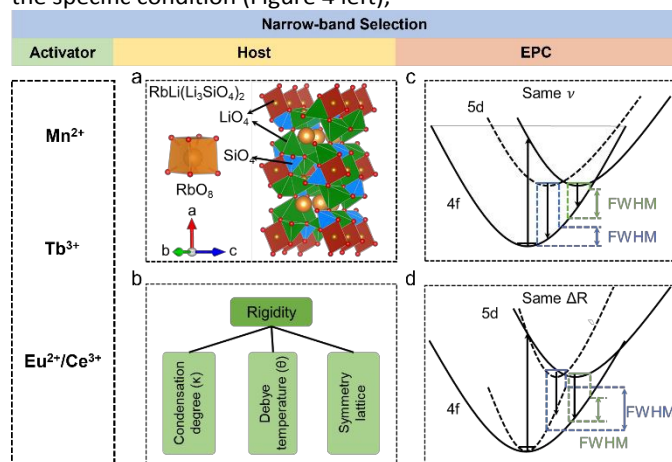**Figure 3.** (a) The crystal structure of $BaBeSiON_2$ and $BaSi_2O_2N_2$. The coordination polyhedra of BaO_4N_3 and BaO_8 in $BaBeSiON_2$ and $BaSi_2O_2N_2$, respectively. (b) The PL and PLE spectra of $BaBeSiON_2:Eu^{2+}$. (c) The variation diagram from Sr_2LiAlO_4 to $Sr_2LiAl_{0.6}Ga_{0.4}O_4$. (d) The PLE spectrum and the PL spectra of $Sr_2LiAl_{1-x}Ga_xO_4:Eu^{2+}$ (x = 0.2, 0.25, 0.3, 0.35 and 0.4). Reproduced with permission from ref. 72. Copyright 2024, Wiley and ref. 73. Copyright 2021, Wiley.

Cationic substitution strategy is a common method for luminescent modification, which adjusts the crystal field intensity of activator by changing the local crystal structure. $BaBeSiON_2:Eu^{2+}$ exhibits redshift by substituting Be with Si in $BaSi_2O_2N_2:Eu^{2+}$, which emits blue light (Figure 3a).Every second $(SiON_3)^{7-}$ is replaced by one $(BeN_3)^{7-}$, which results in the substitution of O by N, inducing enhancement of crystal field splitting. The $BaBeSiON_2:Eu^{2+}$ emits green light peaking at 526 nm with FWHM of 45 nm (Figure 3b).[77] The other approach for luminescence modification is selective site occupancy, which changes the doped site or its coordination number by changing the local environment around activators. $Sr_2LiAl_{0.6}Ga_{0.4}O_4:Eu^{2+}$ exhibits green emission with FWHM of 40 nm, which is obtained by substituting Al^{3+} with Ga^{3+} in $Sr_2LiAlO_4:Eu^{2+}$ with green-yellow double peak emission (Figure 3c). The introduction of Ga^{3+} reduces the number of doped sites by compressing one of luminescent sites and reducing occupation, achieving a single peak green emission (Figure 3d).[78] Another special example of luminescent modification is $NaBaB_9O_{15}:Eu^{2+}$, the activator Eu^{2+} occupies aliovalent Na^+ site rather than isovalent Ba^2, showing green emission peaking at 515 nm with FWHM of 61 nm. The occupancy of Eu^{2+} is regulated by the synthesis related to energetical process, the aliovalent Na^+ site preference occurs after an aging process at low temperature and proved by DFT calculation. Due to the defects induced by aliovalent substitution, this phosphor exhibits good thermal stability and the peak intensity maintains 110% at 500 K compared to 300 K.[79]

2.4 Narrow-band selection

The condition of narrow-band emission should be further discussed. It can be research in three aspects: 1) the activator; 2) the host, and 3) the interaction between the activator and the host. The discussion on activators has been discussed, Mn^{2+}, Tb^{3+}, Ce^{3+} and Eu^{2+} may emits narrow-band green emission at the specific condition (Figure 4 left),

Figure 4. (a) The crystal structure of $RbLi(Li_3SiO_4)_2$ and RbO8 coordination polyhedral. (b) Three criteria (condensation degree, Debye temperature and symmetry lattice) of evaluating the structure rigidity. (c) The configuration coordinate diagram of Eu^{2+} at same phonon frequency. (d) The configuration coordinate diagram of Eu^{2+} at same Stokes shift.

the two latter cases will be discussed in detail here. The host materials with high rigidity and high symmetry more likely exhibit narrow-band emission. The rigid structure can reduce the non-radiation relaxation by limiting the lattice vibration. The symmetry crystal lattice in host can reduce the crystal field splitting, which favors the narrow-band emission (Figure 4a). The rigid of structure can be selected in many aspects (Figure 4b). The κ represents the degree of condensation, which relates to the rigidity of the materials, higher κ represents higher rigidity, the rigidity can be compared by comparing the value of κ, the acknowledged high rigidity UC_4C_4-type has high κ = 1 (AB/X, as mentioned above). However, the connection of the structural framework is different to each other. Some are three-dimensional connections, which are relatively simple, while others are not, thus the rigidity of them is difficult to compare. Debye temperature (θ) is proposed to compare rigidity, which is obtained by theory calculation and experiment, the high rigidity usually exhibits high θ.[80–82] The θ of phosphors higher than that of commercial phosphor $Y_3Al_5O_{12}$ (YAG, θ = 726 K) usually is regarded as high rigid materials.[83] Moreover, the lattice doped by the activator with high symmetry more likely exhibits narrow-band emission due to the small lattice distortion. The interaction between the activator and the host materials is the interaction between transition electron and the lattice vibration (phonon), which is described as electron-phonon coupling (EPC). Intense EPC can induce the non-radiative transition (the transition electron releases energy as the heat), and this non-radiative transition results in the spectral broadening. The strength of EPC can't be directly compared, the equation and diagram are displayed to discuss the EPC. The Huang-Rhys factor (S) and Stokes shift (ΔR) are fitted by temperature-dependent to compare the EPC, as show in the following equation:

$$\Delta R = \sqrt{\frac{2hS}{h\nu}} \qquad \text{equation (3)}$$

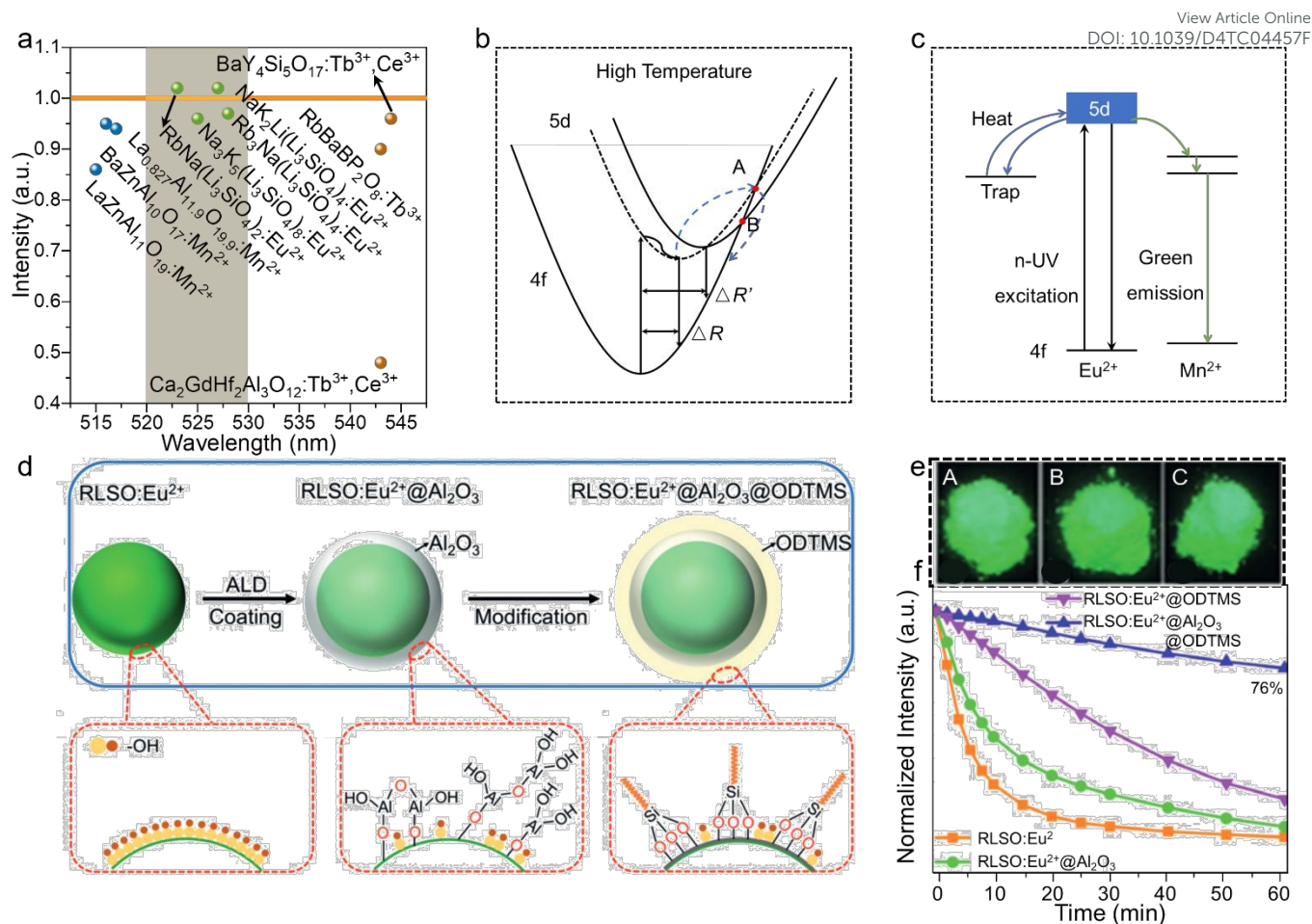$$FWHM^2 = 8ln2S(h\nu)^2 \coth\left(\frac{h\nu}{2kT}\right) \qquad \text{equation (4)}$$

$$FWHM = 2\sqrt{ln2\Delta Rh\nu} * \sqrt{\coth\frac{h\nu}{2kT}} \qquad \text{equation (5)}$$

where S is the Huang-Rhys factor, $h\nu$ is the vibrational phonon energy, ν is the phonon frequency, k is the Boltzmann constant and the T is the temperature.

It is obvious that the FWHM is depended on the ΔR or S, which is related to crystal structure relaxation and ν, as shown in the equation (3). Moreover, configuration coordinate diagram can be used to intuitive display the effect of phonons on electrons. Take the configuration coordinate diagram of Eu^{2+} as example, when the ν is same (same parabolic shape) at different crystal structure relaxation (Figure 4c), smaller ΔR conducts the narrower FWHM. When the ΔR is same at different ν, smaller ν (parabola with large opening) conducts the narrower FWHM (Figure 4d).

Figure 5. (a) The wavelength (nm) and relative luminescence intensity of LZAO:Mn^{2+}, BZAO:Mn^{2+}, LAO:Mn^{2+}, RN:Eu^{2+}, N$_3$K$_5$:Eu^{2+}, R$_3$N:Eu^{2+}, NK$_2$L:Eu^{2+}, RBBPO:Tb^{3+}, BYSO:Tb^{3+},Ce^{3+}, and CGHAO:Tb^{3+},Ce^{3+} at 150 °C compared to the 30 °C. (b) The configuration coordinate diagram of Eu^{2+} at high temperature. (c) The energy level diagram of Eu^{2+}, Mn^{2+} and trap, and the electron transition process between them. (d) The process from RLSO:Eu^{2+} to covered by the Al$_2$O$_3$ and the hydrophobic surface modification with ODTMS. (e) The photographs of RLSO:Eu^{2+} (A), RLSO:Eu^{2+}@Al$_2$O$_3$ (B) and RLSO:Eu^{2+}@Al$_2$O$_3$@ODTMS (C). (f) The normalized intensity of RLSO:Eu^{2+} , RLSO:Eu^{2+}@Al$_2$O$_3$ and RLSO:Eu^{2+}@Al$_2$O$_3$@ODTMS after immersing in water at different time. Reproduced with permission from ref. 81. Copyright 2020, Wiley.
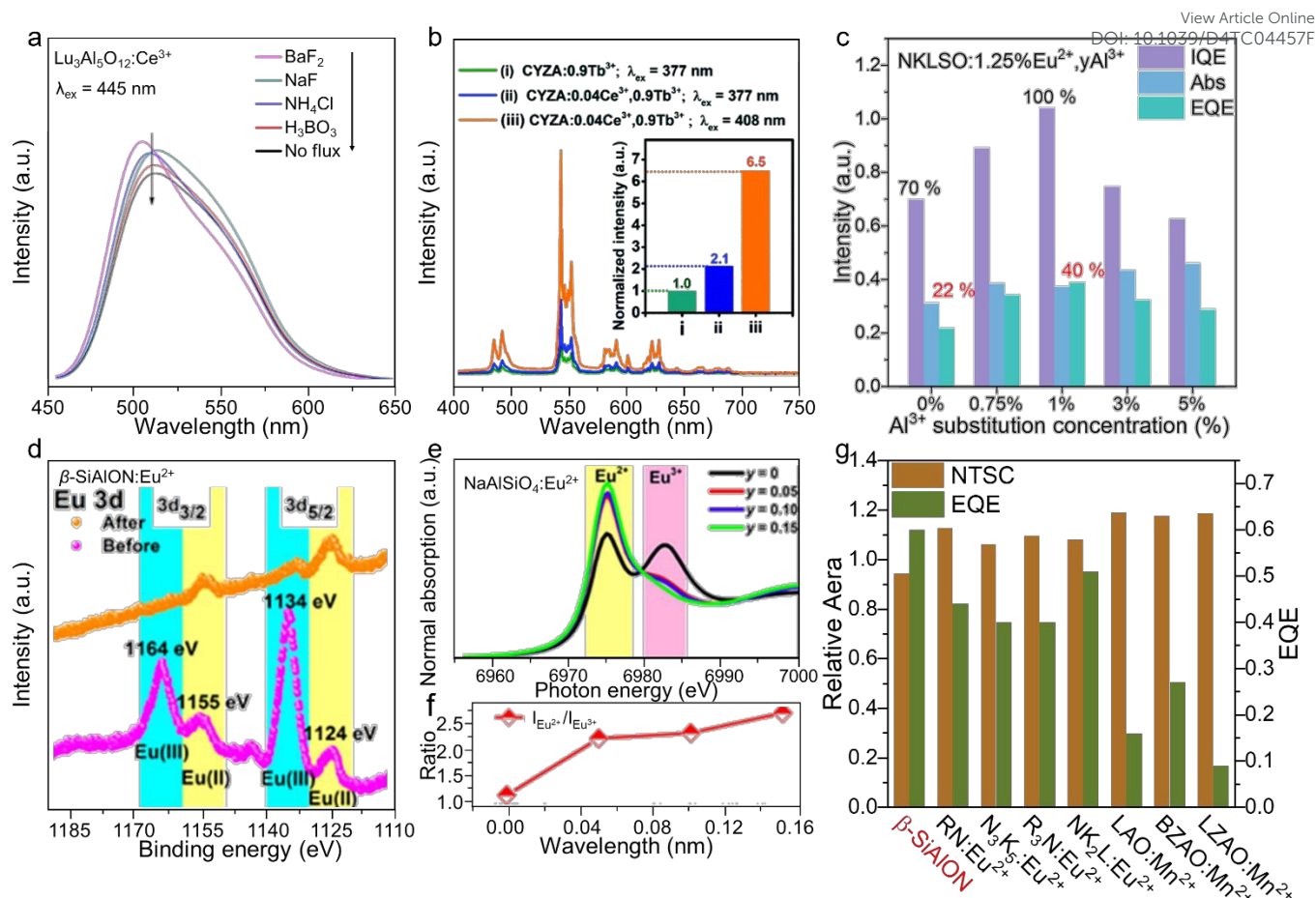
3. Performance enhancement of green-emitting phosphor

3.1 Thermal stability improvement

The other property related to the rigidity and EPC of the host materials is luminescence thermal stability. After long working time, the heating effect of phosphor becomes a noteworthy problem, which should be further solved.[80] A phosphor with good thermal stability can maintain high brightness at high temperature, which should be further developed. A group of green-emitting phosphors LaZnAl$_{11}$O$_{19}$:Mn^{2+} (LZAO:Mn^{2+}), BaZn$_{10}$O$_{17}$:Mn^{2+} (BZAO:Mn^{2+}), La$_{0.827}$Al$_{11.9}$O$_{19.9}$:Mn^{2+} (LAO:Mn^{2+}), RbNa(Li$_3$SiO$_4$)$_2$:Eu^{2+} (RN:Eu^{2+}), Na$_3$K$_5$(Li$_3$SiO$_4$)$_8$:Eu^{2+} (N$_3$K$_5$:Eu^{2+}), Rb$_3$Na(Li$_3$SiO$_4$)$_4$:Eu^{2+} (R$_3$N:Eu^{2+}), NaK$_2$Li(Li$_3$SiO$_4$)$_4$:Eu^{2+} (NK$_2$L:Eu^{2+}), RbBaBP$_2$O$_8$:Tb^{3+} (RBBPO:Tb^{3+}). BaY$_4$Si$_5$O$_{17}$:Tb^{3+},Ce^{3+} (BYSO:Tb^{3+},Ce^{3+}) and Ca$_2$GdHf$_2$Al$_3$O$_{13}$:Tb^{3+},Ce^{3+} (CGHAO:Tb^{3+},Ce^{3+}) doped by Mn^{2+},

Eu^{2+} and Tb^{3+} were selected to compared the thermal stability and peak wavelength (Figure 5a). The crossed aera of yellow aera (peak position from 520 to 530 nm) and orange aera (relative integrated intensity maintains 100% at 150 °C) represents green-emitting phosphors with appropriate peak position and excellent thermal stability. The attenuation of PL intensity generally comes from the increase of non-radiative transition and EPC with increasing temperature. Normally, the structure with high rigidity usually exhibits the good thermal stability, the limitation of the lattice vibration can effectively reduce non-radiation induced by the heating effect. Take the configuration coordinate diagram of Eu^{2+} at high temperature as example, the ΔR at high temperature is larger than that at room temperature, which represents that the larger FWHM at high temperature. Limiting the EPC of phosphors can effectively reduce the ΔR and FWHM (Figure 5b). Selecting the highly rigid structure contributes to directionally select the phosphors withgood thermal stability, the condition of selecting structure with high rigidity has been discussed above.
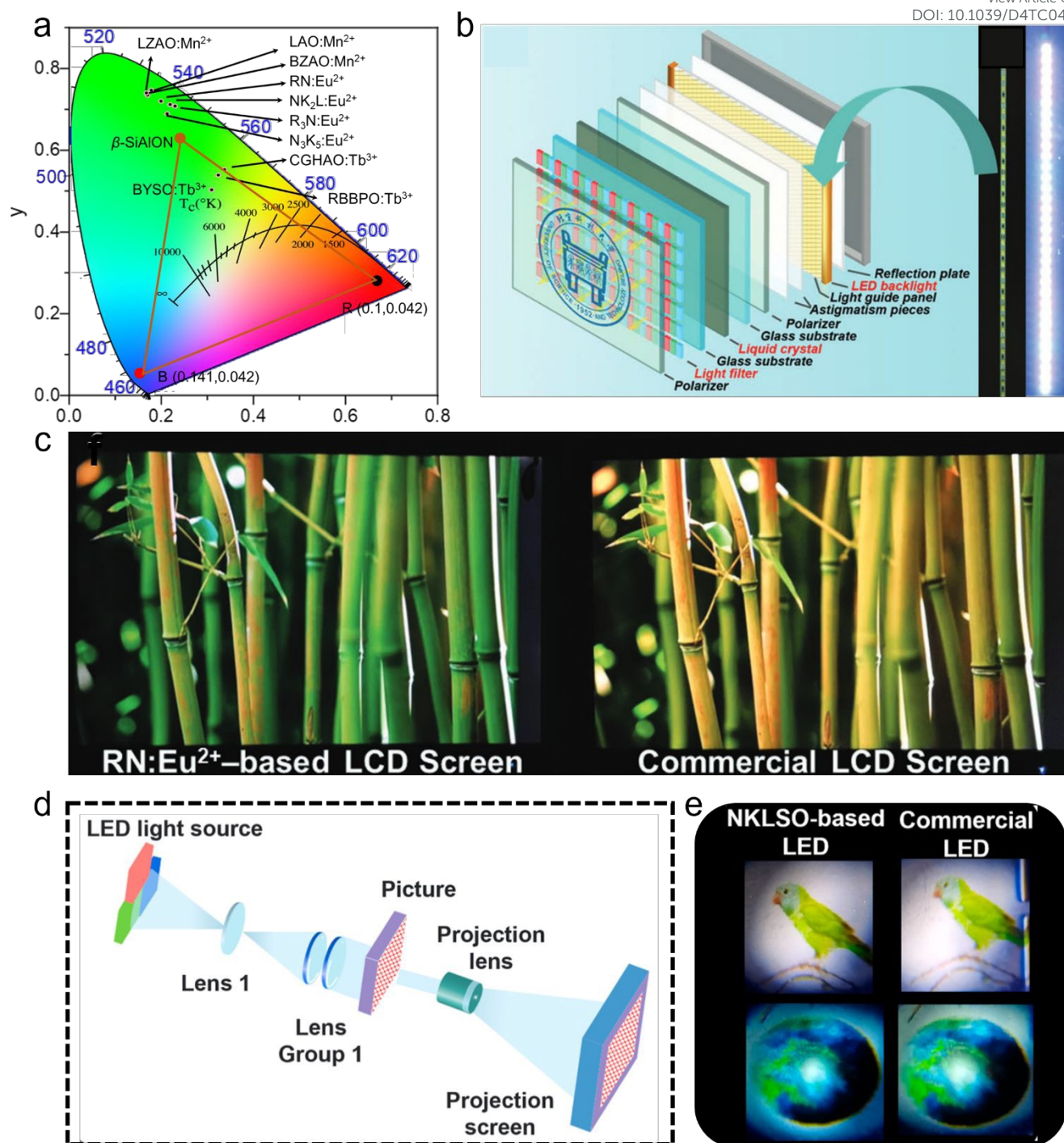
Figure 6. (a) The PL spectra of $Lu_3Al_5O_{12}:Ce^{3+}$ with different flux. (b) The PL spectra of $CYZA:Tb^{3+}$, $CYZA:Tb^{3+},Ce^{3+}$. (c) The IQE, EQE and Abs of $NKLSO:Eu^{2+}$. (d) The high-resolution XRS spectra of Eu 3d before and after post-annealing process. (e) The normalized Eu L_3-edge XANES spectra of $NaAlSiO_4:Eu^{2+},yLi^+$. (f) The quantity curve of Eu^{3+} versus Eu^{2+} (I_{Eu2+}/I_{Eu3+}) of $NaAlSiO_4:Eu^{2+},yLi^+$. (g) The NTSC and EQE of β-SiAlON, $LZAO:Mn^{2+}$, $BZAO:Mn^{2+}$, $LAO:Mn^{2+}$, $RN:Eu^{2+}$, $N_3K_5:Eu^{2+}$, $R_3N:Eu^{2+}$ and $NK_2L:Eu^{2+}$. Reproduced with permission from ref. 90. Copyright 2014, Elsevier, ref. 91. Copyright 2019, Royal Society of Chemistry, ref. 26. Copyright 2023, American Chemical Society, ref. 94. Copyright 2018, American Chemical Society and ref. 95. Copyright 2019, Science.

Typical UCr_4C_4-type phosphors with high rigidity exhibit good thermal stability (Table 1), all of them maintains over 95% integrated intensity at 150 °C. The other way to enhance the thermal stability is to construct a trap level. Part of excited state electrons are captured by trap level in the transition, then return to the ground state, emitting light.[84] Cation heterovalent substitution can induce the vacancy or oxygen defects, which is used to store the energy and enhance the thermal stability. The cation generated the defects comes from two ways, doped heterovalent activator ions and the cation of host. $Na_{1.6}Al_{11}O_{17}:Eu^{2+},Mn^{2+}$ induces oxygen vacancies by replacing Eu^{2+} with Na^+, achieving the anti-thermal quenching, through releasing energy from traps after heating (Figure 5c). Moreover, the emission spectrum of that is regulated to the green light (λ_{em} = 510 nm) with FWHM of 27 nm and reaches high IQE/EQE of 81.8%/55.4%.[84,85] For practical application in daily life, expect for the heating effect during the work-time, the other situation should get more attention, such as high humidity and high working current. UCr_4C_4-type phosphors with excellent luminescent properties suffer from the weak humid stability due to the existence of alkalimetal ions Li, Na, K, Rb, Cs, and the challenge of practical application focus on enhancing the humid

stability. $RbLi(Li_3SiO_4)_2:Eu^{2+}$ ($RLSO:Eu^{2+}$) emits green light with excellent thermal stability (103%@150°C), however, it easily forms RbOH, LiOH and Li_2SiO_3 after reacting with water. Xia's group coats the amorphous Al_2O_3 and hydrophobic octadecyltrimethoxysilane (ODTMS) (Figure 5d) on the surface to enhance the moisture-resistant property of $RbLi(Li_3SiO_4)_2:Eu^{2+}$, the intensity maintains 76% and shows intense green light after being submerged for one hour (Figure 5e and f).[86] The laser-driven solid-state white light source is one of the future research hotspot due to the high brightness, small size, etc.[87] However, the luminescence saturation induced by high-power hinders the use of normal phosphors, the phosphors with high-power-resistant property should be further developed.[88,89] The green-emitting ceramic used for laser diode (LD) should have excellent thermal stability and thermal conductivity, commercial green-emitting ceramic $Lu_3Al_5O_{12}:Ce^{3+}$ ($LuAG:Ce^{3+}$) has been developed as phosphor-in-silica glass to enhance the high-power-resistant property.[90,91] There are few researches on other green-emitting ceramics, which should be further explored. The color purity is a comprehensive index to evaluate the spectrum width, which presents vividness of color.

Figure 7. (a) The color gamut of green-emitting β-SiAlON + blue chip + red-emitting KSF:Mn^{4+}, and the color coordinates of LZAO:Mn^{2+}, BZAO:Mn^{2+}, LAO:Mn^{2+}, RN:Eu^{2+}, N$_3$K$_5$:Eu^{2+}, R$_3$N:Eu^{2+}, NK$_2$L:Eu^{2+}, RBBPO:Tb^{3+}, BYSO:Tb^{3+},Ce^{3+} and CGHAO:Tb^{3+},Ce^{3+}. (b) The LCD prototype (left) and the backlight-1 fabricated by the WLED-1 (right, blue chip + RN:Eu^{2+} green-emitting and KSF:Mn^{4+} red-emitting phosphors). (c) The LCD screen lightened by backlight-1 (left) and backlight-2 (right, blue chip + YAG:Ce^{3+} yellow-emitting and KSF:Mn^{4+} red-emitting phosphors). (d) The prototype and projection mechanism of projector. (e) The photographs of WLED-2 (left, blue chip + N$_3$K$_5$:Eu^{2+} green-emitting and KSF:Mn^{4+} red-emitting phosphors) and WLED-3 (right, blue chip + (Sr,Ba)$_2$SiO$_4$:Eu^{2+} green-emitting and KSF:Mn^{4+} red-emitting phosphors). Reproduced with permission from ref. 65. Copyright 2019, Wiley and ref. 26. Copyright 2023, American Chemical Society.

The narrower the spectrum of phosphor is, the closer to main wavelength is, and the higher the color purity will be. Hence, the color purity should be calculated from the CIE chromaticity coordinates of the narrow-band green-emitting phosphors. The

emission band of the phosphors will broaden at high temperature, the FWHM and peak position at different temperature are compared to discuss the strength of non-radiative relaxation. The color drift is only compared using the

CIE color coordinates, however, the relationship between the peak broadening and the emitting color is rarely noticed. The change of color purity with increasing temperature can be discussed in depth to show the effect of temperature on the luminescence color and color draft in practical application.

3.2 Quantum efficiency enhancement

Quantum efficiency is a vital factor for commercialization of phosphors, the phosphors with high quantum efficiency can reduce energy consumption and save cost.[92] The research on improving QE has been widely concerned and studied, and many methods have been tried to improve QE such as 1) adding flux, 2) constructing energy transfer, 3) substituting cation and 4) adding charge compensator. The addition of fluxes (H_3BO_3, BaF_2 and Li_2CO_3 etc.) can help to melt the raw material and reduce the sintering temperature.[93–95] Samples at lower sintering temperatures reduce defects and increase crystallinity, thus can help to reduce the energy loss and enhance the QE. Moreover, the addition of fluxes may remove impurities during the sintering process though the vaporization of the fluxes. $Lu_3Al_5O_{12}:Ce^{3+}$ effectively enhances the intensity after adding the fluxes, as shown in the Figure 6a.[96] The single activator in the host may exhibit weak luminescence and low QE, the energy transfer by overlapping spectra is designed to enhance the QE. Adding the sensitizer with broadband absorption is an efficient method to achieve energy transfer which can stimulate the luminescence of activator by transfers the excitation energy to the excitation of the activator. Co-doped Ce^{3+} and Tb^{3+} in $Ca_2YZr_2(AlO_4)_3$ (CYZA) green-emitting phosphor has higher IQE of 56% than that of 26% in Tb^{3+}-doped CYZA due to the energy transfer between excitation band of Tb^{3+} and emission band of Ce^{3+} (Figure 6b).[97] The enhancement of QE by cation substitution can be mechanistically explained as the effect of the crystal fields. The change of crystal field directly influences the strength of that, symmetry and coordination number, these changes can affect energy level structure of the activators and enhance the QE. Na^+ replacing the Rb^+ in $Rb_4(Li_3SiO_4)_4:Eu^{2+}$ ($R_4LSO:Eu^{2+}$) forms $Rb_3Na(Li_3SiO_4)_4:Eu^{2+}$ ($R_3NLSO:Eu^{2+}$), the IQE/EQE of that is effectively improved from 70.5%/28.7% to 85.3%/40.4%.[73] The defect and oxygen vacancy induced by heterovalently substitution may reduce QE, the charge compensator is added to balance the charge. $NKLSO:Eu^{2+}$ efficiently improves the IQE/EQE from 70%/22% to 100%/40% after adding charge compensator Al^{3+} compensated the Na^+ heterovalently substituted by Eu^{2+} (Figure 6c). There is a special example Eu^{2+}, the rare earth ion (RE) normally exists at trivalent ion RE^{3+}, hence, the Eu^{2+}-doped phosphors suffers a reduction process. The proportion of the Eu^{2+}/Eu^{3+} significant decides the quantum of the Eu^{2+}-doped phosphors. A lot of methods were used to enhance QE and decrease the ratio of Eu^{3+}, such as adding the reducing materials into the raw materials and using the graphite crucible or carbon paper in the sintering process.[98,99] A simple post-annealing process in reducing N_2/H_2 atmosphere were used to reducing the Eu^{3+} to Eu^{2+} in commercial $β$-SiAlON, the EQE was enhanced from 38.4% to 71.3%.[100] The Eu^{2+} content of that can be compared by X-ray photoelectron spectroscopy (XPS) spectra, it is obvious that the Eu^{2+} intensity of XPS spectra enhanced after post-annealing process (Figure 6d). Substitution of cation for enhancing QE usually changes the local environment of lattice, then applies the effect to activator. $NaAlSiO_4:Eu^{2+}$ enhances the IQE from 75% to 86% by replacing Al^{3+} by Li^+, the Li atom at vacancy of Na is easily help Eu^{3+} to reduce as Eu^{2+}, at same time,

the incorporation of Li^+ changes the site of Eu^{2+} and tunes them emission peak from yellow to green.[101] Eu L_3-edge XANES spectra can directly compare the ratio of Eu^{2+}/Eu^{3+}, it can be seen that the Eu^{2+} content increase with the increasing Li^+ (Figure 6e and 6f). The QE is not only related to the structure of phosphors, but also related to the sintering temperature and time. Long sintering time is conducive to large crystal size and few defects. The relative high sintering temperature also can enhance the crystallinity and reduce the defects. The low number of defects can enhance QE. Suitably prolong the sintering temperature and increasing the sintering time are the feasible ways to enhance QE.

4. Application

Many efficient strategies were used to get the narrow-band green-emitting phosphors, which combines the lattice and band – gap engineering with the local structure and spectrum analysis to design new highly efficient green-emitting phosphors. The application of narrow-band green-emitting phosphors is way to verify the practicality of that, a lot of application modes are exhibited, showing the application prospect of narrow-band green-emitting phosphor.[102,103]

High-definition display is focused owing to the growing demand, the wider gamut can show more colorful picture. The commercial WLED used for display is fabricated by blue chip covered by narrow-band green-emitting $β$-SiAlON phosphor and red-emitting $KSF:Mn^{4+}$ phosphor, and it has gamut of 94% NTSC. The gamut of that decided by the color coordinates of $β$-SiAlON and $KSF:Mn^{4+}$, the wide-band emission of $β$-SiAlON limits the development of gamut (Figure 7a, red triangle). The color gamut is compared which consists of blue chip + $KSF:Mn^{4+}$ phosphor + green-emitting phosphor of $LZAO:Mn^{2+}$, $BZAO:Mn^{2+}$, $LAO:Mn^{2+}$, $RN:Eu^{2+}$, $N_3K_5:Eu^{2+}$, $R_3N:Eu^{2+}$, $NK_2L:Eu^{2+}$, $RBBPO:Tb^{3+}$, $BYSO:Tb^{3+},Ce^{3+}$ and $CGHAO:Tb^{3+},Ce^{3+}$. The gamut of them is extend except phosphors doped by Tb^{3+}, which also prove that Tb^{3+} is not suitable for activator in display due to the multiple emission peaks (Figure 7a). The potential narrow-band green-emitting phosphor with good performance used in novel WLED for display will replace $β$-SiAlON and extend the gamut. The WLED-1 extend the gamut to NTSC of 124%, which is fabricated by blue chip + $La_{0.827}Al_{11.9}O_{19.09}:Mn^{2+}$ ($LAO:Mn^{2+}$) green-emitting and $K_2TiF_6:Mn^{4+}$ (KTF) red-emitting phosphors, larger than that fabricated by $β$-SiAlON with NTSC of 94%.[104] Xia's group developed a LCD prototype (blue chip + $RN:Eu^{2+}$ + KSF) to verify the practicability of $RN:Eu^{2+}$, showing the more vivid picture than commercial LCD screen (blue chip + YAG + KSF) (Figure 7b and 7c).[70] $NKLSO:Eu^{2+}$ + KSF phosphors covered on the blue chip is fabricated as WLED for projection prototype with NTSC of 106%, exhibiting more colorful pictures than commercial LED (blue chip + $(Sr,Ba)_2Si_2O_4:Eu^{2+}$ + KSF) (Figure 7d and 7e).[29]

More than that, the green-emitting phosphor also can be applied in solid state lighting with high CRI, traditional commercial lighting device is fabricated by n-UV chip covered YAG yellow-emitting phosphor.[105,106] However, the commercial WLED device has low CRI, the color will be displayed incorrectly and it is not healthy for the eyes. To increase CRI, a new strategy

used the n-UV chip covered by bule, green and red-emitting phosphors is explored, and the full-spectrum lighting is further developed by extra added phosphors which can cover the gap between blue, green and red phosphors. The WLED exhibits high Ra of 93.5 and the color coordinate is (0.357, 0.353), which is fabricated by n-UV chip covered $Sr_2Ga_2SiO_7$:1% and 5% Eu^{2+} (SGSO:1% and 5% Eu^{2+}) yellow-green phosphor, the $Ba_{0.5}Sr_{1.5}Ga_2SiO_7$:$Eu^{2+}$ (BSGSO:Eu^{2+}) as green phosphor and $Sr_2Si_5N_8$:Eu^{2+} red phosphor.[107]

5. Perspectives

In this review, we summarized the selection of activator and host, modulation of luminescence, improvement of quantum efficiency (QE) and thermal stability and application of green-emitting phosphors in recent years. The activators were selected from Mn^{2+}, Tb^{3+}, Ce^{3+} and Eu^{2+} due to their emission in the visible region. Three methods for selection of host, single particle diagnosis approach, high-throughput density functional theory (DFT) calculation and mineral-inspired prototype evolution, are used to directional search green-emitting phosphors. We discussed a variety of ways to achieve luminescence modulation, enhancing the thermal stability and QE. Finally, multiple application modes such as display device and projector are fabricated to exhibits the larger color gamut and more vivid picture.

However, there is much to improve for high-quality green-emitting phosphors in future. The future development direction of green-emitting phosphor should be based on wide gamut, and developing the PL intensity, QE, thermal stability. Compared to halide perovskite phosphors, traditional inorganic oxide phosphors have disadvantages, such as relative wide emission band and large particle sizes resulted from limited solution processing, limiting its further development. Three aspects that may guide the future direction of green-emitting phosphor development are shown here.

1) The exploration of green-emitting phosphors will aim to ultra-narrow-band emission (narrower than 20 nm) with blue light excitation, high QE, better thermal stability, smaller particle size without the loss of QE. The enhancement to the width, QE, thermal stability of that has been discussed previously and lots of approach have been explored, it will be explored in the foreseeable future to meet these requirements. However, the method for smaller particle size is lacking, the future direction to breakthrough is getting small particle size green-emitting phosphor that can solution processing, using for mini-LED or Micro-LED.

2) Another aspect is to enhance theoretical study of luminescence mechanism. The emission peak and width of green-emitting phosphors have been studied a lot, however, the specific luminescence phenomenon such as abnormal negative thermal quenching and different luminescence in similar structure have not been analyzed in depth. The future research may pay more attention to mechanism, electron structure correlation and band gap of that. Moreover, the

screening of crystal database will be established to select high-quality green-emitting phosphors. It will be more easily to explored new phosphors without going through a tedious human process. Not only that, the theoretical calculation module should be established, which can meet the needs of customization such as specific wavelength, bandwidth, band gap or thermal quenching rate with increasing temperature. The researchers can easily select the corresponding phosphors and test them by using theoretical calculation module.

3) The present research of green-emitting phosphors usually aims to exceed one or two properties by synthesizing new phosphors, and ignore the comprehensive performance. For example, compared to the commercial β-SiAlON, the research of green-emitting phosphor always focuses on the narrower-band, ignores the lifetime and persistent high QE after long worktime. Whereas, it is difficult to explore a perfect new phosphor, we should improve the existing phosphors by available ways. Future development of green-emitting phosphors can be achieved by upgrading existing phosphors to commercial availability.

Conflicts of interest

There are no conflicts to declare.

Acknowledgements

Notes and references

1   F. Farooq, S. Shin, J. Y. Lee, J. Kyhm, G. Kang, H. Ko and H. S. Jang, *ACS Appl. Mater. Interfaces*, 2024, **16**, 38221–38230.
2   B. Zhang, Z. Lu, H. Zhang, W. Li, J. Zhuang, C. Hu, Y. Liu, B. Lei and X. Zhang, *J. Mater. Chem. C*, 2024, **12**, 8852–8860.
3   M. Zhao, Q. Zhang and Z. Xia, *Mater. Today*, 2020, **40**, 246–265.
4   K. Han, J. Jin, X. Zhou, Y. Duan, M. V. Kovalenko and Z. Xia, *Adv. Mater.*, 2024, **36**, 2313247.
5   X. Zhou, M. Yang, C. Shen, L. Lian, L. Hou and J. Zhang, *Nano Lett.*, 2024, **24**, 3719–3726.
6   L. Yang, H. Du, J. Li, Y. Luo, X. Lin, J. Pang, Y. Liu, L. Gao, S. He, J.-W. Kang, W. Liang, H. Song, J. Luo and J. Tang, *Nat. Commun.*, 2024, **15**, 6240.
7   A. M. Srivastava, M. G. Brik, C.-G. Ma, W. W. Beers, W. E. Cohen and M. Piasecki, *J. Phys. Chem. Lett.*, 2024, **15**, 4175–4184.
8   Qu M., Zhang S., Duan J., Dai H., Xuan T., Xie R.-J. and Li H., *Chin. J. Lumin.*, 2024, **45**, 1399–1409.
9   Y. Zhai, D. Zhou, P. Jing, D. Li, H. Zeng and S. Qu, *J. Colloid Interface Sci.*, 2017, **497**, 165–171.
10 S. Zhang, F. Ma, J. Jiang, Z. Wang, R. T. K. Kwok, Z. Qiu, Z. Zhao, J. W. Y. Lam and B. Z. Tang, *Angew. Chem. Int. Ed.*, 2024, **63**, e202408586.

11   J. Chen, Y. Guo, B. Chen, W. Zheng, X. Zhang, X. Wei, Y. Cao, H. Suo and F. Wang, *Adv. Opt. Mater.*, 2024, **12**, 2400147.

12   G. H. Lee, K. Kim, Y. Kim, J. Yang and M. K. Choi, *Nano-Micro Lett.*, 2023, **16**, 45.

13   X. Yu, X. Yang, H. Zhang, K. Liu and J. Yu, *Matter*, 2024, **7**, 2490–2506.

14   Liu C., Wei C., Luo X., Sun Z., Xu B. and Zeng H., *Chin. J. Lumin.*, 2024, **45**, 1410–1430.

15   T. Xuan, S. Guo, W. Bai, T. Zhou, L. Wang and R.-J. Xie, *Nano Energy*, 2022, **95**, 107003.

16   Y. Lu, Y. Xu, S. Chen, J. Lin, J. Zhu, S. Wang, Y. Zheng, F. Huang and D. Chen, *J. Lumin.*, 2022, **248**, 118952.

17   W. Niu, X. Xie, Z. Chen, R. Sun, Y. Li, S. Wang, Y. Zhang, C. Yang and A. Tang, *Adv. Opt. Mater.*, 2024, **12**, 2400762.

18   X. He, T. Li, Z. Liang, R. Liu, X. Ran, X. Wang, L. Guo and C. Pan, *Adv. Opt. Mater.*, 2024, **12**, 2302726.

19   S. Liu, L. Li, X. Qin, R. Du, Y. Sun, S. Xie, J. Wang, M. S. Molokeev, S. Xi, J.-C. G. Bünzli, L. Zhou and M. Wu, *Adv. Mater.*, 2406164.

20   M.-H. Fang, J. L. Jr. Leaño and R.-S. Liu, *ACS Energy Lett.*, 2018, **3**, 2573–2586.

21   S. Gai, P. Gao, K. Chen, C. Tang, Y. Zhao, J. Wei, Y. Zhang, M. S. Molokeev, M. Xia and Z. Zhou, *Adv. Opt. Mater.*, 2024, **12**, 2302870.

22   Z. Xu, Z. Zhang, H. Sun and Q. Zhang, *J. Chin. Soc. Rare Earths*, 2024, **42**, 901–908.

23   S. A. Khan, N. Z. Khan, Y. Xie, M. Rauf, I. Mehmood, J. Ahmed, S. M. Alshehri, M. A. M. Khan, J. Zhu and S. Agathopoulos, *J. Lumin.*, 2022, **243**, 118650.

24   Y. Zhu, Y. Liang, S. Liu, H. Li and J. Chen, *Adv. Opt. Mater.*, 2019, **7**, 1801419.

25   Q. Liu, P. Dang, G. Zhang, H. Lian, Z. Cheng, G. Li and J. Lin, *Chem. Mater.*, 2024, **36**, 1763–1772.

26   V. Rajagopal, R.-J. Xie and R. Nagaraj, *J. Lumin.*, 2022, **252**, 119356.

27   S. Wang, H. Wu, Y. Fan, Q. Wang, T. Tan, R. Pang, S. Zhang, D. Li, L. Jiang, C. Li and H. Zhang, *Chem. Eng. J.*, 2022, **432**, 134265.

28   L. Zheng, L. Zhang, L. Fang, H. Wu, H. Wu, G.-H. Pan, Y. Yang, Y. Luo, Z. Hao and J. Zhang, *Adv. Opt. Mater.*, 2024, **12**, 2301480.

29   Y. Wan, P. Dang, D. Liu, Q. Zhang, Y. Wei, H. Lian, G. Li and J. Lin, *Chem. Mater.*, 2023, **35**, 10702–10712.

30   S. Li, R. Tian, T. Yan, Y. Guo, Y. Liu, T.-L. Zhou, L. Wang and R.-J. Xie, *Mater. Today*, 2023, **70**, 82–92.

31   K. Zhang, W. Fan, T. Yao, S. Wang, Z. Yang, J. Yao, L. Xu and J. Song, *Adv. Mater.*, 2024, **36**, 2310521.

32   Z. Li, N. Yang, S. Ding, Z. Zhang, W. Huang, Z. Ye, M. Zhao and J. Shi, *J. Mater. Sci. Technol.*, 2025, **205**, 159–167.

33   S.-Y. Zhu, D. Zhao, S.-J. Dai, R.-J. Zhang and L.-Y. Shi, *CrystEngComm*, 2022, **24**, 2966–2975.

34   X. Zhu, S. Zhang and S. Ye, *J. Phys. Chem. Lett.*, 2024, **15**, 2804–2814.

35   S. Li, W. Hu, M. G. Brik, S. Lian and Z. Qiu, *Inorg. Chem. Front.*, 2022, **9**, 3224–3232.

36   E. H. Song, Y. Y. Zhou, Y. Wei, X. X. Han, Z. R. Tao, R. L. Qiu, Z. G. Xia and Q. Y. Zhang, *J. Mater. Chem. C*, 2019, **7**, 8192–8198.

37   X. Zhu, S. Zhang and S. Ye, *J. Phys. Chem. Lett.*, 2024, **15**, 2804–2814.

38   P. Dang, H. Lian and J. Lin, *Adv. Opt. Mater.*, 2023, **11**, 2202511.

39   W. Wang, H. Yang, M. Fu, X. Zhang, M. Guan, Y. Wei, C. C. Lin and G. Li, *Chem. Eng. J.*, 2021, **415**, 128979.

40   H. R. Girisha, B. R. Radha Krushna, K. Manjunatha, H.-H. Chiu, M.-K. Ho, S. Y. Wu, B. Subramanian and H. Nagabhushana, *Mater. Today Sustain.*, 2023, **24**, 100493.

41   X. Liu, H. Cheng, B. Yue, Z. Wen, Y. Jin, G. Liu, S. Liu, D. Li, J. Wang, W. Yu and X. Dong, *J. Colloid Interface Sci.*, 2024, **666**, 162–175.

42   B. C. Jamalaiah, P. S. Khan, N. Madhu, P. Gawas, V. Nutalapati, A. S. Narayana Reddy and G. V. L. Reddy, *Ceram. Int.*, 2022, **48**, 28927–28934.

43   Zhang H., Ding Q., Chen F., Miao Y., Yu D. and Zhang D., *Chin. J. Lumin.*, 2024, **45**, 1114–1122.

44   J. Chang, Y. Wang, Z. Zhang, D. Guo, P. Zhao, N. Wang, Z. Wang, L. Li, P. Li and H. Suo, *Laser Photonics Rev.*, 2023, **17**, 2300542.

45   G. W. Jung and K. Park, *J. Mater. Sci. Technol.*, 2021, **82**, 187–196.

46   Y. Chen, J. Wang, X. Zhang, G. Zhang, M. Gong and Q. Su, *Sens. Actuators B Chem.*, 2010, **148**, 259–263.

47   S. Yang, W. Sun, Q. Xu, C. Yang, S. Zhang and M. Jiao, *Spectrochim. Acta. A. Mol. Biomol. Spectrosc.*, 2023, **292**, 122402.

48   Z. Huang, Z. Lyu, S. Shen, S. Wang, Z. Yang, C. Chen and H. You, *Inorg. Chem.*, 2024, **63**, 6362–6369.

49   X. Huang, J. Liang, S. Rtimi, B. Devakumar and Z. Zhang, *Chem. Eng. J.*, 2021, **405**, 126950.

50   J. Liang, L. Sun, S. Wang, Q. Sun, B. Devakumar and X. Huang, *J. Alloys Compd.*, 2020, **836**, 155469.

51   Y. Xiao, Z. Hao, L. Zhang, X. Zhang, G.-H. Pan, H. Wu, H. Wu, Y. Luo and J. Zhang, *J. Mater. Chem. C*, 2018, **6**, 5984–5991.

52   Y. Lin, H. Lin, P. Wang, J. Xu, Y. Cheng and Y. Wang, *Laser Photonics Rev.*, 2024, 2400995, 10.1002/lpor.202400995.

53   Y. Guo, Y. Wang, Y. Lu, L. Luo, W. Li and P. Du, *Laser Photonics Rev.*, 2024, 2400183, 10.1002/lpor.202400183.

54   Y. Du, T. Seto, W. Liu, Y. Wang and X. Ma, *Adv. Opt. Mater.*, 2024, **12**, 2302183.

55   B. Guo, M. Wen, H. Tang, S. Lishik, X. Fan, G. Zhang and J. Fan, *Laser Photonics Rev.*, 2024, **18**, 2300838.

56   S. Tian, P. Fen, X. Qiao and Y. Wang, *J. Chin. Soc. Rare Earths*, 2024, **42**, 894–900.

57   Z. Xia, Z. Xu, M. Chen and Q. Liu, *Dalton Trans.*, 2016, **45**, 11214–11232.

58   T. Takeda, N. Hirosaki, S. Funahashi and R.-J. Xie, *Mater. Discov.*, 2015, **1**, 29–37.

59   X. Luo and R.-J. Xie, *J. Rare Earths*, 2020, **38**, 464–473.

60   T. Takeda, N. Hirosaki, S. Funahshi and R.-J. Xie, *Chem. Mater.*, 2015, **27**, 5892–5898.

61   H. Ming, Y. Zhou, M. S. Molokeev, C. Zhang, L. Huang, Y. Wang, H.-T. Sun, E. Song and Q. Zhang, *ACS Mater. Lett.*, 2024, **6**, 1790–1800.

62   M. Liao, Z. Mu, Q. Wang, X. Zhang, H. Dong, M. Wen and F. Wu, *J. Alloys Compd.*, 2020, **837**, 155084.

63   C. Park, J.-W. Lee, M. Kim, B. D. Lee, S. P. Singh, W. B. Park and K.-S. Sohn, *Inorg. Chem. Front.*, 2021, **8**, 4610–4624.

64   R. Shafei, D. Maganas, P. J. Strobel, P. J. Schmidt, W. Schnick and F. Neese, *J. Am. Chem. Soc.*, 2022, **144**, 8038–8053.

65   R. Lu and J. Sun, *Materials*, 2023, **16**, 5053.

66   Q. Zhang, X. Ding, H. Wang, B. Liu and Y. Wang, *J. Mater. Chem. C*, 2023, **11**, 15366–15375.

67   J. Sun, W. Zhu, B. Zhang, F. Huang, L. Hu, H. Ma, R. Ye, Y. Hua and S. Xu, *Opt. Mater.*, 2023, **146**, 114529.

68   F. Ruegenberg, A. García-Fuente, M. Seibald, D. Baumann, G. Hoerder, T. Fiedler, W. Urland, H. Huppertz, A. Meijerink and M. Suta, *Adv. Opt. Mater.*, 2023, **11**, 2202732.

69   J. Sun, M. Zhou, B. Zhang, Y. Hua, F. Huang, H. Ma, R. Ye and S. Xu, *Dalton Trans.*, 2022, **51**, 11703–11712.

70   H. Liao, M. Zhao, Y. Zhou, M. S. Molokeev, Q. Liu, Q. Zhang and Z. Xia, *Adv. Funct. Mater.*, 2019, **29**, 1901988.

71   X. Wang, X. Huang, M. Zhao, P. A. Tanner, X. Zhou and L. Ning, *Inorg. Chem.*, 2022, **61**, 7617–7623.

72   M. Zhao, H. Liao, L. Ning, Q. Zhang, Q. Liu and Z. Xia, *Adv. Mater.*, 2018, **30**, 1802489.

73   M. Liao, Q. Wang, Q. Lin, M. Xiong, X. Zhang, H. Dong, Z. Lin, M. Wen, D. Zhu, Z. Mu and F. Wu, *Adv. Opt. Mater.*, 2021, **9**, 2100465.

74   M.-H. Fang, C. O. M. Mariano, K.-C. Chen, J.-C. Lin, Z. Bao, S. Mahlik, T. Lesniewski, K.-M. Lu, Y.-R. Lu, Y.-J. Wu, H.-S. Sheu, J.-F. Lee, S.-F. Hu, R.-S. Liu and J. P. Attfield, *Chem. Mater.*, 2021, **33**, 1893–1899.

75   M. Liao, F. Wu, J. Wang, D. Zhu, X. Zhang, H. Dong, Z. Lin, M. Wen and Z. Mu, *ACS Appl. Mater. Interfaces*, 2022, **14**, 47892–47901.

76   J. Xu, C. He, L. Zeng, G. Li, C. Li, H. Lin, J. Liu, L. Zhou, J. Yang and J. Tang, *J. Lumin.*, 2024, **268**, 120398.

77   T. Giftthaler, P. Strobel, V. Weiler, A. Haffner, A. Neuer, J. Steinadler, T. Bräuniger, S. D. Kloß, S. Rudel, P. J. Schmidt and W. Schnick, *Adv. Opt. Mater.*, 2024, **12**, 2302343.

78   J. Qiao, Y. Zhou, M. S. Molokeev, Q. Zhang and Z. Xia, *Laser Photonics Rev.*, 2021, **15**, 2100392.

79   Y. Zhuo, S. Hariyani, J. Zhong and J. Brgoch, *Chem. Mater.*, 2021, **33**, 3304–3311.

80   H. Zhang, H. Li, C. Liu, H. Jiang, J. Li, Y. Liu, J. He, R. Wang, W. Hu and J. Zhu, *Chem. Eng. J.*, 2024, **490**, 151727.

81   D. Wen, H. Liu, Z. Ma, L. Zhou, J. Li, Y. Guo, Q. Zeng, P. A. Tanner and M. Wu, *Angew. Chem. Int. Ed.*, 2023, **62**, e202307868.

82   S. Hariyani, A. C. Duke, T. Krauskopf, W. G. Zeier and J. Brgoch, *Appl. Phys. Lett.*, 2020, **116**, 051901.

83   J. Brgoch, S. P. DenBaars and R. Seshadri, *J. Phys. Chem. C*, 2013, **117**, 17955–17959.

84   R. Shi, S. Cao, Y. Han, J. Zhang, X. Zhang, S. Liao and S. Lian, *Appl. Mater. Today*, 2022, **29**, 101625.

85   R. Shi, X. Zhang, Z. Qiu, J. Zhang, S. Liao, W. Zhou, X. Xu, L. Yu and S. Lian, *Inorg. Chem.*, 2021, **60**, 19393–19401.

86   M. Zhao, K. Cao, M. Liu, J. Zhang, R. Chen, Q. Zhang and Z. Xia, *Angew. Chem. Int. Ed.*, 2020, **59**, 12938–12943.

87   G. Liu, W. Chen, Z. Xiong, Y. Wang, S. Zhang and Z. Xia, *Nat. Photonics*, 2024, **18**, 562–568.

88   S. Li, Y. Guo and R.-J. Xie, *Acc. Mater. Res.*, 2022, **3**, 1299–1308.

89   S. Li, L. Wang, N. Hirosaki and R.-J. Xie, *Laser Photonics Rev.*, 2018, **12**, 1800173.

90   B. Zhang, J. Zhou, W. Zhu, F. Huang, R. Ye, H. Ma, Y. Hua and S. Xu, *Ceram. Int.*, 2024, **50**, 5868–5876.

91   Y. Zhou, C. Li, J. Ning and F. Tang, *Adv. Opt. Mater.*, 2024, **12**, 2400374.

92   Z. Zhang, Y. Ren, S. Zhang, H. Mu, X. Li and X. Sun, *J. Chin. Soc. Rare Earths*, 2024, **42**, 909–917.

93   Z. Lu, D. Sun, Z. Lyu, S. Shen, X. Zhang, S. Wei, P. Luo, L. Zhou and H. You, *Mater. Today Chem.*, 2023, **34**, 101813.

94   W. Ahn, M. Im and Y. J. Kim, *Mater. Res. Bull.*, 2017, **96**, 254–257.

95   J. Gao, L. Dong, Y. Lin, P. Zhou, X. Ma, J. Hou and Y. Fang, *J. Mater. Chem. C*, 2024, **12**, 7435–7445.

96   Y. Yu, H. Wang, L. Li, Y. Chen and R. Zeng, *Ceram. Int.*, 2014, **40**, 14171–14175.

97   L. Sun, B. Devakumar, J. Liang, S. Wang, Q. Sun and X. Huang, *J. Mater. Chem. C*, 2019, **7**, 10471–10480.

98   Z. Yang, G. Liu, Y. Zhao, Y. Zhou, J. Qiao, M. S. Molokeev, H. C. Swart and Z. Xia, *Adv. Opt. Mater.*, 2022, **10**, 2102373.

99   J. Qiao, S. Zhang, X. Zhou, W. Chen, R. Gautier and Z. Xia, *Adv. Mater.*, 2022, **34**, 2201887.

100   S. Li, L. Wang, D. Tang, Y. Cho, X. Liu, X. Zhou, L. Lu, L. Zhang, T. Takeda, N. Hirosaki and R.-J. Xie, *Chem. Mater.*, 2018, **30**, 494–505.

101   M. Zhao, Z. Xia, X. Huang, L. Ning, R. Gautier, M. S. Molokeev, Y. Zhou, Y.-C. Chuang, Q. Zhang, Q. Liu and K. R. Poeppelmeier, *Sci. Adv.*, 2019, **5**, eaav0363.

102   R.-J. Xie, N. Hirosaki and T. Takeda, *Appl. Phys. Express*, 2009, **2**, 022401.

103   X. Li, W. Feng, F. You, T. Pang, J. Zhu, J. Lin, Y. Fang and D. Chen, *Adv. Opt. Mater.*, 2023, 2302823.

104   C. Zhan, H. Zhu, S. Liang, Y. Huang, Z. Wang and M. Hong, *Inorg. Chem. Front.*, 2024, **11**, 826–836.

105   W. Xia, Q. Zhao, L. Du, F. Du, Y. Zhang, T. Zhang, F. Hao and Z. Tang, *Chem. Eng. J.*, 2024, **484**, 149723.

106   P. He, Y. Li, J. Zuo, B. Zhang, F. Yang, J. Peng, S. Liu, W. Wang, D. Huang, Y. Xiao and X. Ye, *J. Alloys Compd.*, 2024, **985**, 173997.

107   D. Liu, R. Zhao, C. Wang, Z. Liu, J. Zhang, Y. Wang, X. Yu, J. Qiu, X. Xu and Y. Liu, *Mater. Today Phys.*, 2024, **40**, 101325.

Journal of Materials Chemistry C Accepted Manuscript

The authors confirm that the data supporting the findings of this study are available within the article and its supplementary materials.